

4-1-2015

# In-vivo longitudinal MRI study: an assessment of melanoma brain metastases in a clinically relevant mouse model.

Mariama N Henry

Yuhua Chen

Catherine D McFadden

Felicia C Simedrea

Paula J Foster

Follow this and additional works at: <https://ir.lib.uwo.ca/biophysicspub>



Part of the [Medical Biophysics Commons](#)

---

## Citation of this paper:

Henry, Mariama N; Chen, Yuhua; McFadden, Catherine D; Simedrea, Felicia C; and Foster, Paula J, "In-vivo longitudinal MRI study: an assessment of melanoma brain metastases in a clinically relevant mouse model." (2015). *Medical Biophysics Publications*. 68.  
<https://ir.lib.uwo.ca/biophysicspub/68>

# In-vivo longitudinal MRI study: an assessment of melanoma brain metastases in a clinically relevant mouse model

Mariama N. Henry<sup>a,b</sup>, Yuhua Chen<sup>a</sup>, Catherine D. McFadden<sup>a</sup>, Felicia C. Simeanea<sup>c</sup> and Paula J. Foster<sup>a,b</sup>

Brain metastases are an important clinical problem. Few animal models exist for melanoma brain metastases; many of which are not clinically relevant. Longitudinal MRI was implemented to examine the development of tumors in a clinically relevant mouse model of melanoma brain metastases. Fifty thousand human metastatic melanoma (A2058) cells were injected intracardially into nude mice. Three Tesla MRI was performed using a custom-built gradient insert coil and a mouse solenoid head coil. Imaging was performed on consecutive days at four time points. Tumor burden and volumes of metastases were measured from balanced steady-state free precession image data. Metastases with a disrupted blood–tumor barrier were identified from T1-weighted spin echo images acquired after administration of gadopentetic acid (Gd-DTPA). Metastases permeable to Gd-DTPA showed signal enhancement. The number of enhancing metastases was determined by comparing balanced steady-state free precession images with T1-weighted spin echo images. After the final imaging session, ex-vivo permeability and histological analyses were carried out. Imaging showed that both enhancing and nonenhancing brain metastases coexist in the brain, and that most metastases switched from the nonenhancing to the enhancing phenotype. Small

numbers of brain metastases were enhancing when first detected by MRI and remained enhancing, whereas other metastases remained nonenhancing to Gd-DTPA throughout the experiment. No clear relationship existed between the permeability of brain metastases and size, brain location and age. Longitudinal in-vivo MRI is key to studying the complex and dynamic processes of metastasis and changes in the blood–tumor barrier permeability, which may lead to a better understanding of the variable responses of brain metastases to treatments. *Melanoma Res* 25:127–137 Copyright © 2015 Wolters Kluwer Health, Inc. All rights reserved.

*Melanoma Research* 2015, 25:127–137

**Keywords:** balanced steady-state free precession, blood–brain barrier, blood–tumor barrier, brain metastasis, clinically relevant mouse model, gadolinium, melanoma, permeability, 3 T MRI, T1-weighted spin echo

<sup>a</sup>Robarts Research Institute, <sup>b</sup>Department of Medical Biophysics, Western University and <sup>c</sup>London Regional Cancer Program, London, Ontario, Canada

Correspondence to Mariama N. Henry, MSc, 3004 Brimley Dr., Windsor, Ontario, Canada N8R 1M2

Tel: +1 519 735 2207; fax: +1 519 663 3404; e-mail: mhenry43@alumni.uwo.ca

Received 14 March 2014 Accepted 10 November 2014

## Introduction

A common complication among patients with malignant melanoma is metastasis to the brain [1,2]. Patients with metastatic melanoma have a 40–60% risk of developing brain metastases [3]. Autopsy series reports have shown an incidence of melanoma brain metastasis ranging from 17.5 to greater than 90% [3–6]. Compared with other primary tumors such as lung and breast cancer, melanoma has a greater tendency to metastasize to the brain [3,7]. The prognosis for patients with melanoma brain metastasis remains dismal, with a median survival of 1–2 months without treatment [8–10] and 4–6 months with treatment [8,11], and a 1-year survival rate in less than 13% of patients [12]. Chemotherapeutics are limited in their ability to cross the blood–brain barrier (BBB) and consequently have little efficacy in the treatment of brain metastases [7,13].

The local BBB associated with brain tumors is referred to as the blood–tumor barrier (BTB) [14–17]. Several studies have described significant heterogeneity in the permeability of the BTB associated with individual brain metastases [18,19]. Lockman *et al.* [18] showed that the

BTB of breast cancer brain metastases in mice exhibited significant heterogeneity in permeability to dextran and that permeability was unrelated to the size or to the morphology of the metastases. Zhang and colleagues examined brain metastases produced by eight human cancer cell lines and reported that permeability to sodium fluorescein varied depending on the tumor type and was related to tumor morphology and size. Small compact metastases were not permeable until they reached 0.2 mm<sup>2</sup> and diffuse metastases were permeable only when they coalesced to form a large mass [20]. These studies were based on ex-vivo experiments conducted at specific endpoints and provide only a snapshot of the permeability status of metastases. MRI has also been used to evaluate BBB integrity *in vivo* [21–23]. Gadolinium contrast agents such as gadopentetic acid (Gd-DTPA) are routinely used in MRI to demonstrate BBB breakdown [19,24–27]. Gadolinium is impermeable to an intact BBB; however, extravascular enhancement in MRI images after administration of Gd-DTPA is indicative of a leaky BBB or increased permeability [28]. Percy *et al.* [19] used Gd-DTPA-enhanced MRI to

evaluate BBB permeability and tumor burden in a mouse model of breast cancer metastasis to the brain.

Only a few studies have carried out a longitudinal analysis of melanoma brain metastases [29–31], yet to date none have performed a detailed assessment of enhancing and nonenhancing melanoma brain metastases with respect to the factors influencing the changes in permeability. In this study, longitudinal MRI was used to characterize a clinically relevant model of melanoma brain metastases; the BTB integrity and the total metastatic burden were determined at four time points during the development of brain metastases. Factors such as volume, brain location, and age were investigated to determine their potential influence on the changes in metastatic tumor permeability.

## Materials and methods

### Animal model

The human metastatic melanoma A2058 cell line was purchased from the American Type Culture Collection and cultured at 37°C in a 5% CO<sub>2</sub> atmosphere in Dulbecco's Modified Eagle Medium containing 10% fetal bovine serum (Gibco; Invitrogen, Burlington, Ontario, Canada). Nude female mice (nu/nu) that were 6–8 weeks old were used (Charles River Laboratories, Saint Constant, Quebec, Canada) in accordance with an approved animal use protocol from the Western University – University council on animal care. A 28.5 gauge insulin syringe was used to inject 100 µl of 50 000 A2058 cells (contained in Hank's balanced salt solution) into the left ventricle of the beating mouse heart [19,32]. Mice were weighed and monitored weekly for signs of health or sickness.

### Magnetic resonance imaging

Mice were imaged using a 3 T GE MR750 MRI clinical scanner (General Electric, Milwaukee, Wisconsin, USA) equipped with a custom-built gradient coil insert (maximum gradient coil strength = 500 mT/m and peak slew rate = 3000 T/m/s) and a solenoid radiofrequency (RF) mouse head coil (inner diameter = 1.5 cm). Before scanning, mice were anesthetized with 3% isoflurane for induction and 1–2% isoflurane for maintenance (in 100% oxygen). For longitudinal analysis, two imaging sequences were used on consecutive days at four different time points after cell injection: days 21/22, days 24/25, days 27/28, and days 30/31. On the first day, before scanning, mice were injected intraperitoneally with 200 µl of undiluted Gd-DTPA (Magnevist; Schering, Whippany, New Jersey, USA). T1-weighted spin echo (T1wSE) images were acquired 60 min after Gd-DTPA injection using the following parameters: resolution = 156 × 156 × 500 µm, TR/TE = 600/20 ms, signal averages = 12, receiver bandwidth = ± 15.63 kHz, and scan time = 15 min. On the second day, balanced steady-state free precession (bSSFP) images were acquired using the following parameters: resolution 100 × 100 × 200 µm, TR/TE = 8/4 ms, flip angle = 35°, signal averages = 2, receiver bandwidth = ± 41.67 kHz, RF phase cycles = 8, and scan time = 30 min.

### Image analysis

OsiriX image software (open source) was used for image visualization and analysis. bSSFP images were used to count the number of metastases and measure the volumes of individual metastases within the whole brain at each time point. Volume measurements were obtained using a manual trace method where tumor borders were manually outlined in each image slice and a final algorithm was computed to obtain a three-dimensional tumor volumetric measurement (mm<sup>3</sup>). T1wSE images were used to determine which metastases were enhanced (leaky BTB) after Gd-DTPA administration. T1wSE images were viewed alongside bSSFP images at all four imaging time points. Enhancing metastases were defined as those with an increase in signal intensity compared with the surrounding mouse brain tissue, in regions in which bSSFP revealed a metastasis. Metastases classified as nonenhancing were not visible on T1wSE images but were visualized on bSSFP images. Parenchymal metastases were defined as those located within and surrounded by brain tissue, as well as having no contact with the surfaces of the brain. Metastases classified as meningeal were described as having at least one side adjacent to the surface of the brain. Verification of meningeal metastases was performed using a reslice tool in OsiriX, which further classified meningeal metastases as originating from either the pia (leptomeninges) or dura mater according to the bSSFP MRI appearance.

### Histology

After Gd-DTPA permeability analysis, mice ( $n=4$ ) anesthetized with 3% isoflurane received 1.5 mg Dextran Texas Red (Invitrogen/Molecular Probes, Eugene, Oregon, USA) by tail vein injection. After 20 min, the mice were perfused with 4% paraformaldehyde and their brains were removed and placed overnight in increasing concentrations of sucrose (10, 20, and 30%) for cryoprotection. Mice brain tissues were embedded in Tissue-Tek optimal cutting temperature medium (Sakura, Saskatchewan, Canada). Frozen sections were cut with a cryostat (Leica Microsystems, Concord, Ontario, Canada) at 20 µm. Mice ( $n=3$ ) that did not receive dextran perfusions were perfused only with 4% paraformaldehyde. Their brain tissues were embedded in paraffin and cut with a microtome (Leica Microsystems) at a thickness of 10 µm, followed by hematoxylin and eosin (H&E) staining. Dextran leakage, visualized as red fluorescence (595 nm excitation, 615 nm emission), was imaged using a fluorescence Zeiss Axio Imager A1 microscope (Zeiss, Oberkochen, Germany) with a Retiga Exi (QImaging, Surrey, BC, Canada) digital camera for capturing images. Image Pro Plus software (Media Cybernetics, Inc., Rockville, Maryland, USA) was used for histological image editing.

### Statistical analysis

Statistical analyses were carried out using GraphPad Prism software (GraphPad Software, Inc., La Jolla,

California, USA). Comparison of groups (enhancing vs. nonenhancing brain metastases) at each time point was performed using the Kruskal–Wallis test, followed by the post-hoc test, Dunn’s multiple comparison test. The level of statistical significance was  $P$  less than 0.05.

## Results

### In-vivo magnetic resonance imaging of melanoma brain metastases

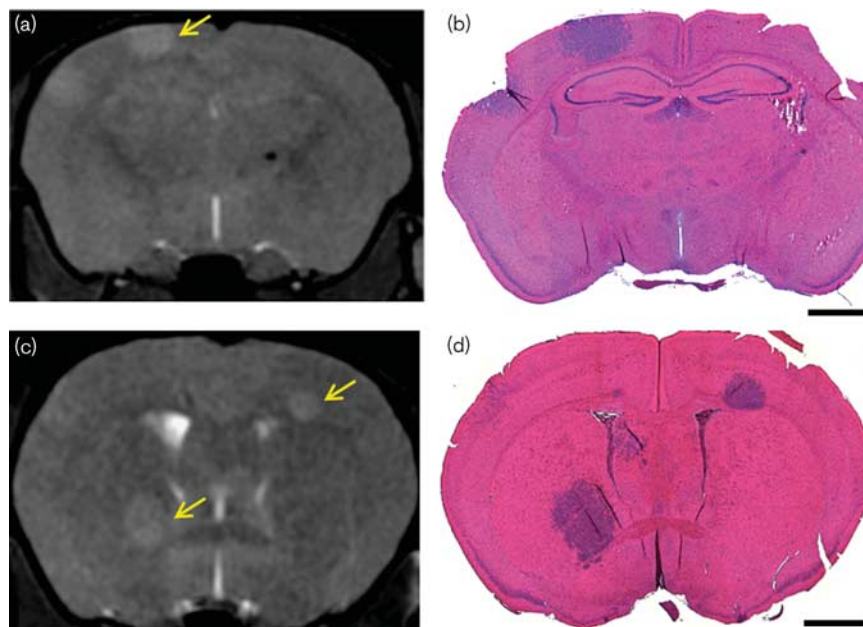
To characterize melanoma brain metastasis a cell injection of 50 000 A2058 human metastatic melanoma cells was delivered intracardially to the mouse brain. This cell injection number produced between three and 23 brain metastases per animal. Meningeal and parenchymal melanoma brain metastases were observed (Fig. 1a and c). The appearance of meningeal and parenchymal metastases in bSSFP images (Fig. 1a and c) was slightly or moderately hyperintense (increase in signal intensity). The corresponding hematoxylin and eosin stain (H&E) histological images (Fig. 1b and d) showed meningeal and parenchymal metastases to be hypercellular lesions.

Hemorrhage was also visualized on bSSFP MRI and H&E staining. The development of hemorrhage (region of low signal intensity) was observed on bSSFP images (Fig. 2b–d, yellow arrows). At day 25, signal loss (Fig. 2b) was observed within a parenchymal metastasis; over time,

this signal hypointensity increased in size. At day 31, visualization of the tumor was obscured by the blooming artifact (Fig. 2d) due to the accumulation of super-paramagnetic species. H&E staining (Fig. 2f and g) revealed the presence of associated hemorrhage within the parenchymal metastasis; hemorrhage is very common in melanoma brain metastases in clinical practice. An isointense (same contrast as background brain tissue) parenchymal metastasis was inconspicuous (Fig. 2a–d, blue arrows) on bSSFP scans but was easily identified on H&E histological images (Fig. 2e, green arrow).

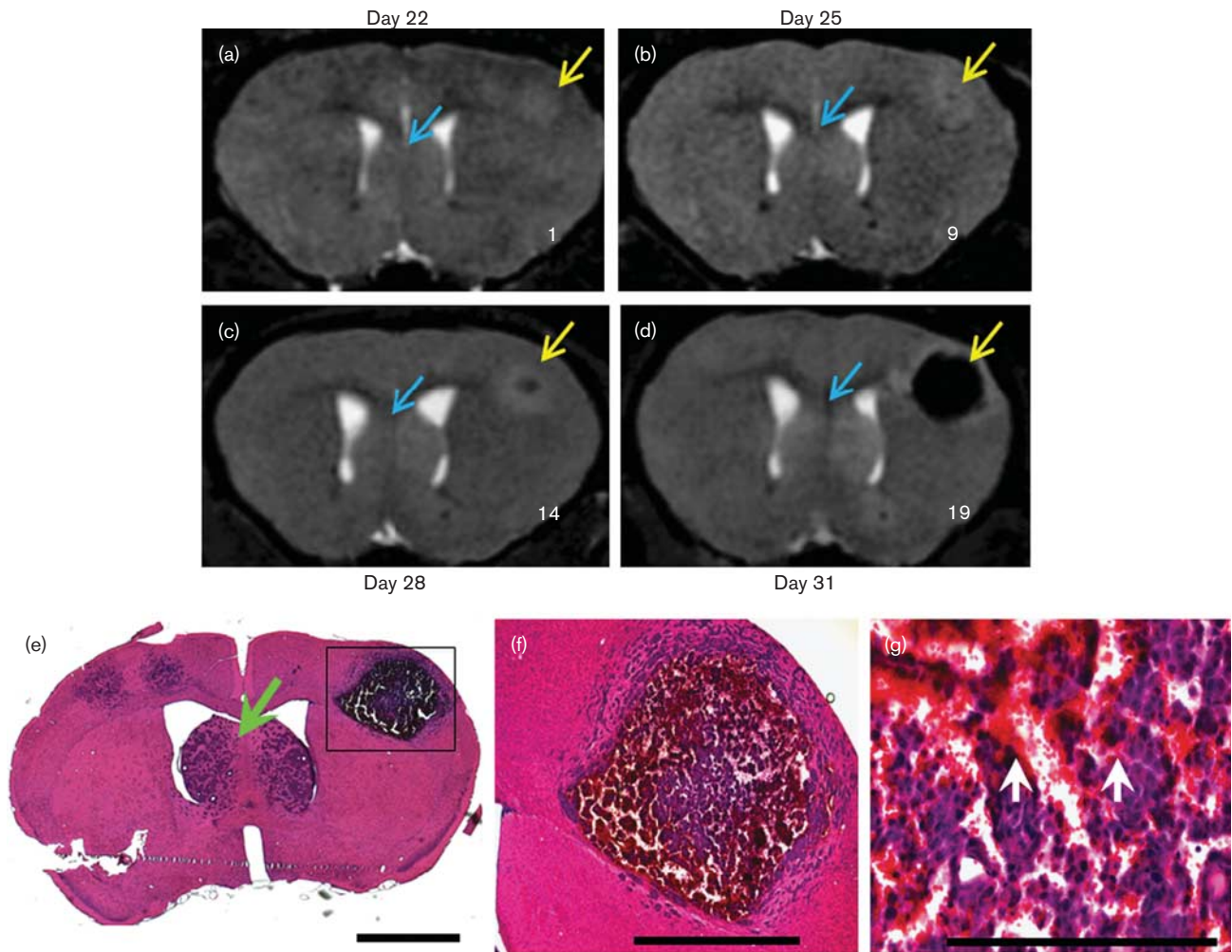
During longitudinal studies, bSSFP MRI enabled early detection of small nonenhancing melanoma brain metastases. An example of the sensitivity of bSSFP toward small nonenhancing metastases is seen in Fig. 3. A single metastasis (Fig. 3c) was visible on bSSFP images at day 25, but not at day 24 with T1wSE images obtained after Gd-DTPA administration (Fig. 3a). The nonenhancing metastasis visible at day 25 (Fig. 3c) was visible as an enhancing metastasis at day 27, after Gd-DTPA administration (Fig. 3b). At day 28, this metastasis had increased in size. During longitudinal analysis, we observed in most cases that, at the early time point, metastases were nonenhancing after Gd-DTPA administration, and thus they are not associated with a disrupted BTB; however, they were detectable on bSSFP images.

Fig. 1



Mouse brain bSSFP MRI and whole-brain histology for A2058 melanoma brain metastases. (a, c) Representative bSSFP images of melanoma brain metastases (yellow arrows). (a) Meningeal metastases (yellow arrow) appear hyperintense relative to the surrounding brain tissue. A signal void (black dot; hypointense signal) is also detected near the middle of the brain in the bSSFP image. (b) H&E-stained histological tissue section showing a hypercellular meningeal metastasis toward the top of the mouse brain. (c) Parenchymal metastases (yellow arrows) appear hyperintense in the brain parenchyma. (d) H&E-stained histological tissue section showing three parenchymal brain lesions; two metastatic parenchymal lesions are hypercellular and appear to be strongly stained with H&E, whereas the other (near the ventricle) appears to be only faintly stained with H&E, which could be due to early stages of tumor development. Scale bars = 250  $\mu$ m. bSSFP, balanced steady-state free precession; H&E, hematoxylin and eosin.

Fig. 2



Hypointense and isointense melanoma mouse brain metastases on bSSFP MRI with H&E histology. (a–d) Representative bSSFP images showing the development of a parenchymal brain metastasis (yellow arrows) in the frontal brain region at four time points. A region of signal hypointensity (low signal intensity) appears over time at the center of the parenchymal metastasis. This metastasis increased in size over time. (d) A blooming artifact obscures visualization of the metastasis at day 31. (a–d) An isointense metastasis (blue arrows) remains inconspicuous in the bSSFP images at all four time points. (e) The isointense metastasis in the bSSFP image is identified in H&E histology (green arrow), scale bar = 250 μm. (f) Inset of metastasis enclosed by a black square in (e) showing the presence of hemorrhage in the H&E-stained section, scale bar = 400 μm. (g) H&E histological image obtained at high-power magnification (×40) showing the presence of blood (white arrows) nested in between and surrounding A2058 melanoma cells, scale bar = 650 μm. Numbers near the lower right corner of each bSSFP image (a–d) refer to the total metastatic burden at each time point. bSSFP, balanced steady-state free precession; H&E, hematoxylin and eosin.

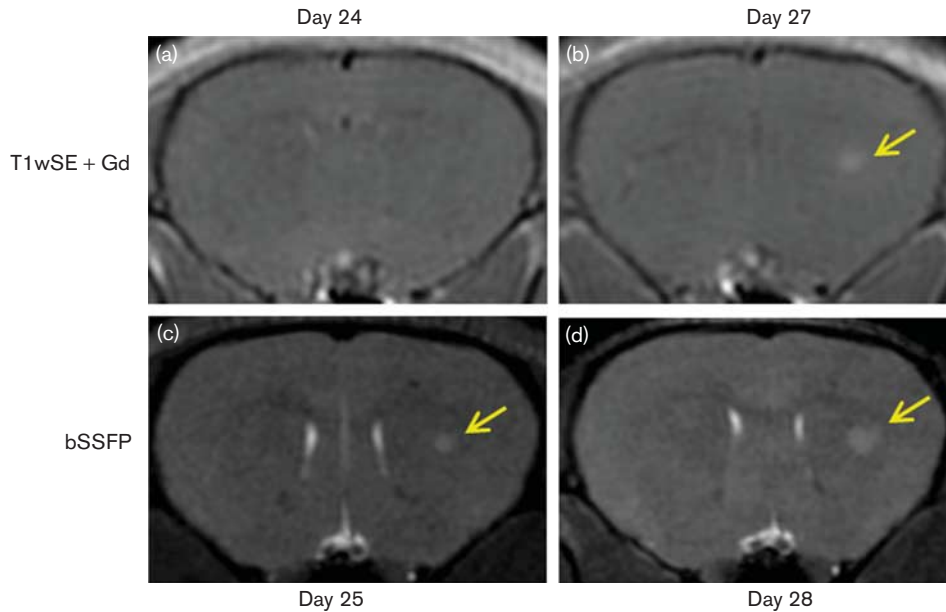
The melanoma brain metastases did not all show enhancement after Gd-DTPA administration at the same time point; rather, they typically changed from non-enhancing to enhancing from one scanning time point to the next. In Fig. 4, T1wSE images obtained after Gd-DTPA administration (Fig. 4a–d) and bSSFP images (Fig. 4e–h) of a mouse brain have been shown. On day 22, a metastasis was visible on the bSSFP image (Fig. 4e); however, it did not appear to be enhancing after Gd-DTPA administration until day 24 (Fig. 4b). At day 27, a new enhancing metastasis was visible near the top of the brain (Fig. 4c) and was also visible on bSSFP images (Fig. 4g and h). At day 31, a third metastasis was detected

by bSSFP (Fig. 4h); however, it was not yet enhancing after Gd-DTPA administration. In general, the number of enhancing metastases in our longitudinal MRI study increased over time. An exception was the case of one mouse that had only nonenhancing brain metastases.

#### Volume, location, and age of enhancing and nonenhancing brain metastases

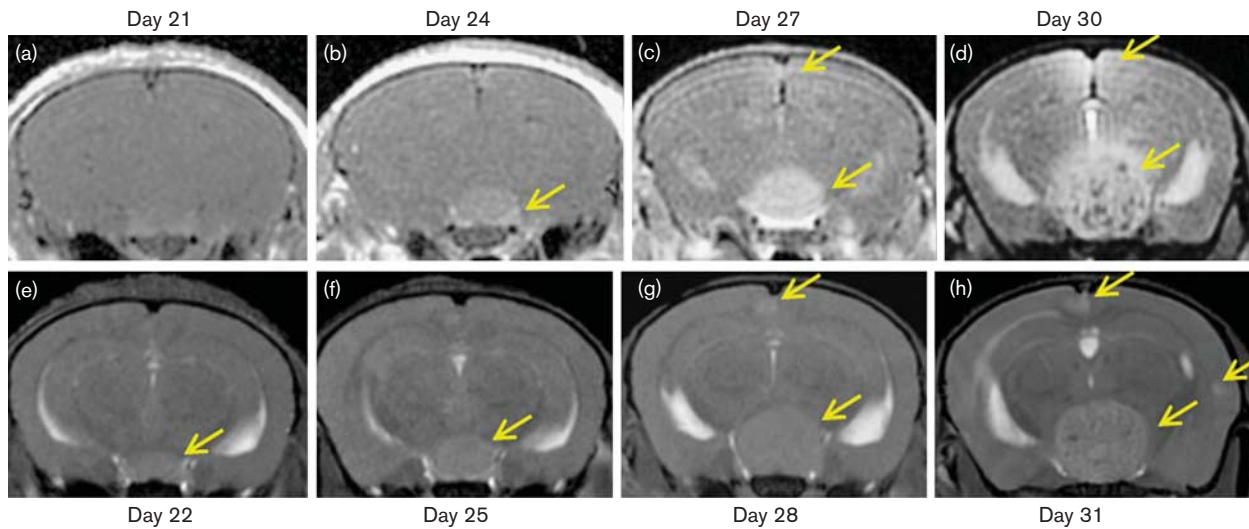
Factors such as volume, brain location, and age of a metastasis were studied to determine whether they had an effect on the permeability of metastases. A wide range of volumes were measured for enhancing and non-enhancing metastases at each time point (Fig. 5a).

**Fig. 3**



Early detection of nonenhancing melanoma brain metastases using bSSFP. Representative T1wSE images obtained after Gd-DTPA administration and bSSFP images in a melanoma brain metastasis mouse model. (a) At day 24, enhancing metastases are not visible after Gd-DTPA administration, but at day 25, a nonenhancing metastasis (yellow arrow) is visible at the early time point using bSSFP MRI. (b) An enhancing metastasis is now visible (yellow arrow) at day 27 after Gd-DTPA administration. (d) At day 28, the metastasis has increased in size. bSSFP, balanced steady-state free precession; Gd-DTPA, gadopentetic acid.

**Fig. 4**



Asynchronous appearances of enhancing and nonenhancing melanoma brain metastases. (a–d) Metastases do not all appear to be permeable to Gd-DTPA at the same imaging time point. Often, they change from a nonenhancing tumor to an enhancing tumor over time. (e) A meningeal brain metastasis (yellow arrow) was detected on bSSFP images at day 22 but was not permeable to Gd-DTPA at day 21. This metastasis was enhancing after Gd-DTPA administration at the next imaging session, on day 24. At day 27, a new enhancing metastasis was visible near the top of the brain and was also visible on bSSFP images. (h) At day 31, a third metastasis is detected by bSSFP, but it is not yet enhancing after Gd-DTPA administration. Yellow arrows = metastases. bSSFP, balanced steady-state free precession. Gd-DTPA, gadopentetic acid.

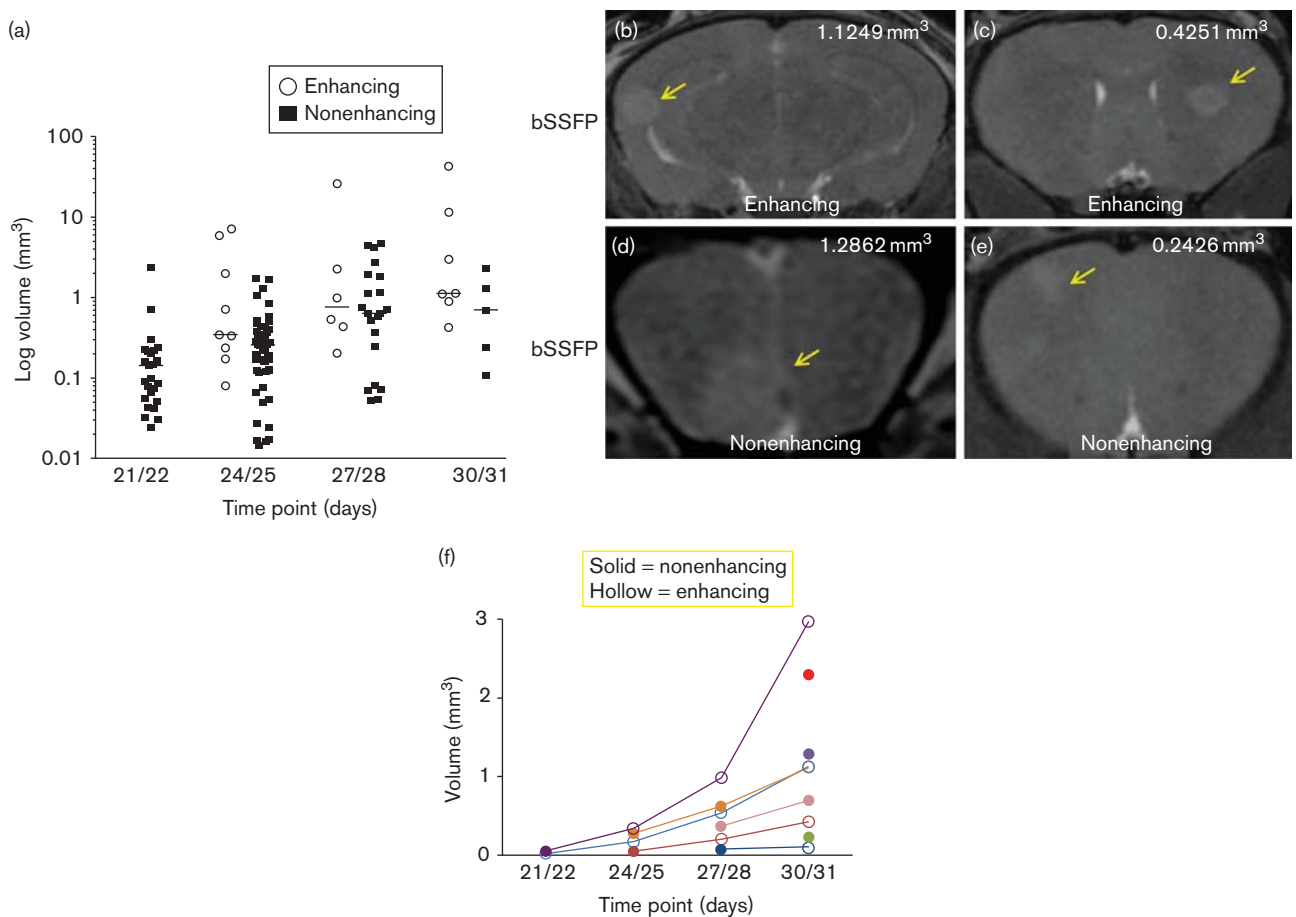
The volume data analyzed suggest that metastasis volume is not a contributor toward changes in permeability, as both small and large metastases were observed as enhancing at days 24, 27, and 30 (Fig. 5a). For instance, the smallest and largest enhancing metastases at days 24, 27, and 30 were 0.0804 and 7.15 mm<sup>3</sup>, 0.204 and 26 mm<sup>3</sup>, and 0.425 and 42.9 mm<sup>3</sup>, respectively. Overall, the volumes of metastases increased over time. However, there was no statistically significant difference ( $P < 0.05$ ) between the volumes of enhancing and nonenhancing metastases at any time point.

Melanoma brain metastases within various regions of the mouse brain (Fig. 5b–e) were also studied. We observed

that enhancing and nonenhancing metastases were dispersed throughout the brains of the mice. Brain location did not have an effect on metastasis volume either, as both large and small lesions were detected throughout the brain (data not shown).

The age of a metastasis did not predict whether a metastasis would become enhancing after Gd-DTPA administration. In Fig. 5f, the patterns of enhancement are illustrated. There are, for example, brain tumors (i) that first appear as an enhancing metastasis and remain as an enhancing metastasis (these are few in number); (ii) that first appear as a nonenhancing metastasis and then switch to an enhancing metastasis at a later imaging

Fig. 5



Enhancement versus volume, brain region and age of metastases. (a) The volumes of enhancing and nonenhancing metastases increased over time. A trend toward increasing volumes was observed. However, no statistical difference ( $P < 0.05$ ) in tumor volumes at each time point was evident. Bars represent medians. (b–e) Representative bSSFP images showing enhancing and nonenhancing metastases in different brain regions. (b, c) Enhancing metastases with their corresponding volumes in the (b) midbrain–hindbrain region and (c) the frontal region, respectively. (d, e) Nonenhancing metastases with their corresponding volumes in (d) the olfactory–frontal region and (e) the frontal region. (f) Patterns of enhancement over time for A2058 melanoma brain metastases. Each colored line and dot shown in (f) represents a different metastasis. Light blue line = metastasis first detected as enhancing and which remained enhancing, pink line = metastasis that never enhanced. Light red, dark blue, and dark purple lines = metastases that first appeared as nonenhancing but changed to enhancing at later time points. Red, green, and light purple dots = late-appearing metastases that were nonenhancing. Hollow circles = enhancing metastases and solid circles = nonenhancing metastases. bSSFP, balanced steady-state free precession.

time point (these constitute the majority of brain metastases); and (iii) that first appear as a nonenhancing metastasis and remain as a nonenhancing metastasis (these are more rare). In no case did we observe an enhancing metastasis switch to a nonenhancing metastasis.

#### **Histology: in-vivo permeability versus ex-vivo permeability**

In-vivo permeability using Gd-DTPA contrast agent (MW 590Da) was compared with ex-vivo permeability using the Dextran Texas Red tracer (MW 3 kDa). Gd-DTPA was selected to assess the in-vivo BBB integrity as it is routinely used clinically to assess BBB integrity. The Dextran Texas Red tracer was selected to assess ex-vivo permeability and to compare our results with those of previously published studies that have also used dextran to assess BBB integrity. In Fig. 6a–d, an example of an enhancing metastasis is shown. This metastasis is clearly visible on both bSSFP images and those obtained on T1wSE after Gd-DTPA administration (Fig. 6a and b). Red fluorescence microscopy (Fig. 6c) for this enhancing metastasis showed evidence of permeability to dextran. Dextran leakage was not homogeneous throughout the enhancing metastasis, implying that some blood vessels may be more permeable than others within this metastasis. H&E histological images (Fig. 6d) for the enhancing metastasis at day 31 showed a hypercellular mass comprising small cell clusters. In Fig. 6e–h, an example of a nonenhancing metastasis is shown. This brain metastasis is detected on the bSSFP image but not on T1wSE images obtained after Gd-DTPA administration. Red fluorescence microscopy (Fig. 6g) for this nonenhancing metastasis showed small punctate regions, confined to vessels, which were permeable to dextran, suggesting that BTB regions within this nonenhancing metastasis were not completely intact (Fig. 6g). H&E histological images for the nonenhancing metastasis (Fig. 6h) showed less hypercellularity, which may indicate that this tumor is in a relatively early stage of development.

#### **Discussion**

In the present study, we have characterized the appearance and size of melanoma brain metastases using MRI. This model of melanoma brain metastases recapitulates many of the MRI and histological features of brain metastases in melanoma patients. These features include: (i) the presence of both parenchymal and meningeal metastases, (ii) hemorrhage, (iii) three to 23 metastases in mice compared with one to 10 in patients, (iv) variable MRI appearance, and (v) rapid growth. Despite our ability to recapitulate much of what is seen in humans, this model presents a limitation because of the fact that the immune-compromised status of the mice may limit the extrapolation of the model to humans. To our knowledge, this is the first study to use 3 T MRI to monitor the development of melanoma brain metastases longitudinally. Metastasis and BTB permeability are dynamic processes and hence longitudinal imaging is

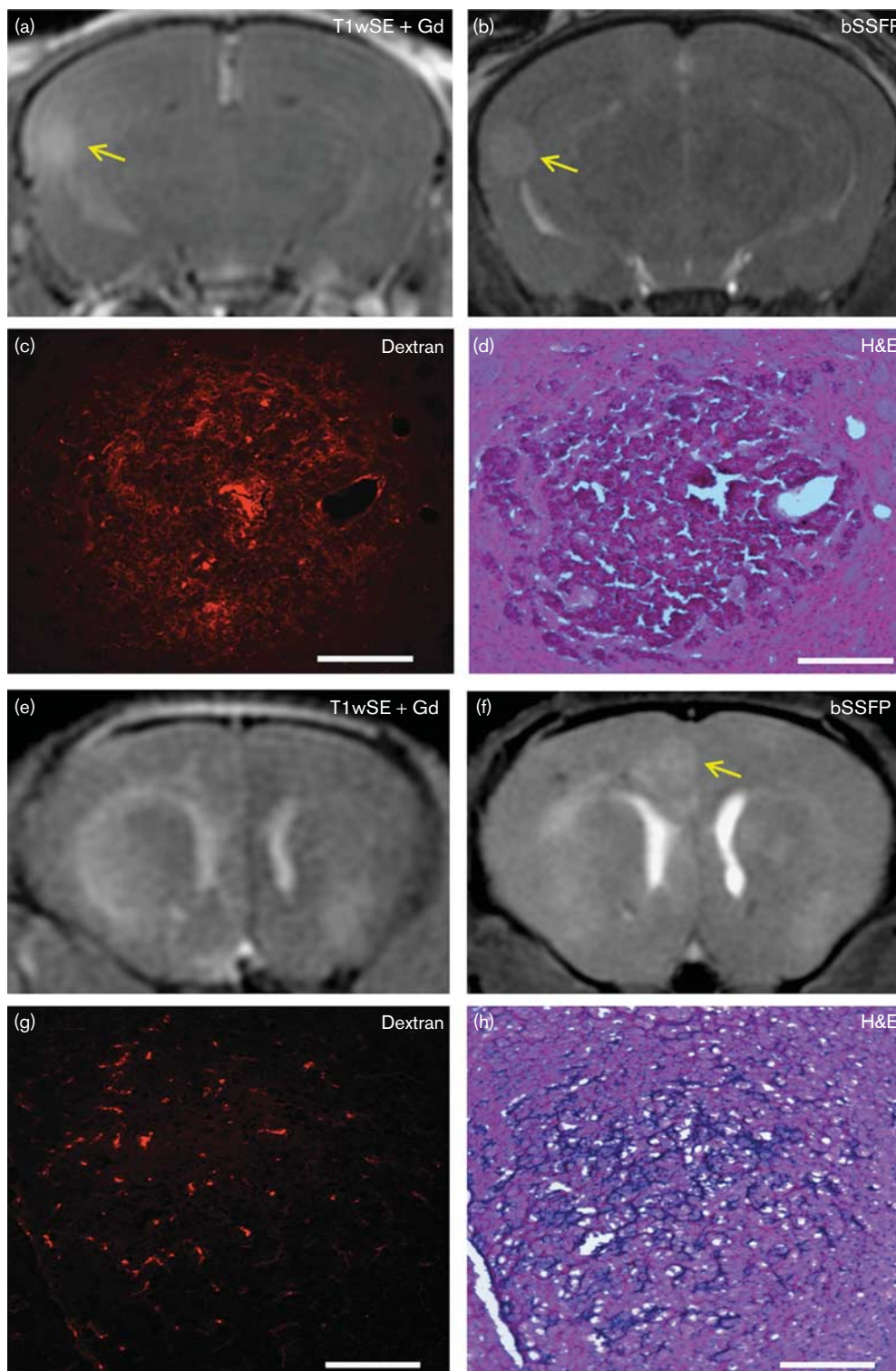
essential to study the development of an altered BBB in metastases.

This is the first report on the use of bSSFP to image melanoma brain metastases. Brain metastases appeared slightly or moderately hyperintense compared with the surrounding brain tissue on bSSFP images, which have contrast related to T2/T1. This could be due to the degree of melanin present and/or hemorrhage, as melanin and methemoglobin, a blood degradation product, both affect the extent of T1 shortening (leading to variations in signal hyperintensity). Occasionally there were metastases that appeared hypointense, more often at late time points, which were likely caused by the presence of blood degradation products such as hemosiderin. Rarely, we identified metastases that were isointense on bSSFP images and were therefore inconspicuous, probably due to simultaneous T1 and T2 shortening or the absence of melanin. The variation in MRI appearances of melanoma brain metastasis in our model is consistent with that reported clinically and is based largely on the degree of melanin and the presence or absence of hemorrhage [33–36].

Our MRI approach allows us to investigate the whole-brain metastasis burden (using bSSFP) and the permeability status (using Gd-DTPA-enhanced T1wSE) of all tumors and thus can be used for the in-vivo evaluation of the response of gadolinium-enhancing and gadolinium-nonenhancing metastases to treatment. There are two important aspects of the BTB in brain metastases. The first relates to tumor detection by MRI. A compromised BTB allows the MRI contrast agent gadolinium to leak into the tissue and this creates signal enhancement in images that are sensitive to it. Clinically, gadolinium is widely used for brain tumor detection. The fact that not all metastases are leaky does not mean that all metastases are detected by this conventional MRI approach. This may also be true in human brain metastasis imaging. bSSFP imaging may be a superior detection method. Second, chemotherapies generally do not work for brain metastases because they cannot cross the BTB. What is important is that we understand more about how the heterogeneity in the permeability of brain metastases is related to drug efficacy. Chemotherapeutics may reach the leakiest of brain tumors but we show here that a significant number of melanoma brain metastases are nonenhancing. Our MRI approach allows us to investigate the whole-brain metastasis burden and the permeability status of all tumors and can be used for the in-vivo evaluation of the response of both gadolinium-enhancing and gadolinium-nonenhancing metastases to treatment.

Others have reported heterogeneity in the permeability of brain metastases. Zhang *et al.* [20] showed through histological analysis that there was variability in the BBB permeability of brain metastases generated in mice from eight different human cancer cell lines (breast, colon,

Fig. 6



Comparison of in-vivo and ex-vivo permeabilities. (a, b) Representative T1wSE images obtained after Gd-DTPA administration and bSSFP images for an enhancing A2058 melanoma brain metastasis (yellow arrows). (c) Ex-vivo permeability showing dextran leakage (red fluorescence) into the tumor interstitial spaces; dextran leakage is not homogeneous throughout the lesion, as some areas have brighter fluorescence compared with other regions. (d) H&E histological images showing a hypercellular morphology for the enhancing metastasis. (e, f) Representative T1wSE images obtained after Gd-DTPA administration and bSSFP images for a nonenhancing A2058 melanoma brain metastasis. A metastasis is only visible in the bSSFP image (f, yellow arrow); (e) no enhancing metastases are visible in the T1wSE images obtained after Gd-DTPA administration. (g) Ex-vivo permeability histology showing small amounts of dextran leakage within the interstitial tissue; bright regions of dextran fluorescence appeared to be confined within blood vessels. (h) H&E histology at day 31 showing little hypercellularity. A2058 melanoma cells also appeared to be more closely associated with the cerebral vasculature, scale bars = 320  $\mu$ m. bSSFP, balanced steady-state free precession; Gd-DTPA, gadopentetic acid; H&E, hematoxylin and eosin.

renal, and melanoma). Lockman *et al.* [18] demonstrated that breast cancer brain metastases in nude mice showed a range of values for passive permeability to the 3 kDa tracer Texas red fluorescent dextran. This work was followed up by an in-vivo MRI study conducted by Percy *et al.* [19] at our laboratory. They showed that no enhancing metastases were visualized at the early time point with T1wSE using Gd-DTPA.

To understand what factors could be involved with changes in permeability, the metastasis size, brain location and age were investigated to observe whether they had any influence on permeability. We found no relationship between location in the brain and enhancement after Gd-DTPA administration. Neither did the age of the metastases nor did the time between cell injection and the imaging time point influence permeability status. However, we cannot exclude the possibility that with more time a 'nonenhancing' tumor may change to an 'enhancing' tumor. Furthermore, size of the metastases increased with time but there was no significant difference in volumes assessed from MRI data of enhancing and nonenhancing metastases at any imaging time point. These findings are very similar to those previously observed by Percy *et al.* [19] for brain metastases due to breast cancer. Lockman *et al.* [18] also reported no clear relationship between the diameter of the brain metastases, measured by histological analysis, and the degree of permeability to dextran. Historically, changes in the integrity of the BTB have been associated with large brain tumors (1–4 mm), which become oxygen and nutrient deprived and develop angiogenic vessels [37, 38]. Our data, however, show that even very small metastases may be leaky. Differences in the specific tracer or contrast agent used, the cell lines, and the timing of the interrogation of tumors may be possible reasons for discrepancies between the results of our study and those of others. Together, all of these studies reveal a complex relationship between biological features of a brain metastasis and BTB permeability.

Several mechanisms of tumor-associated vascularization have been identified, which influence vascular permeability in the brain [39]. The first is angiogenesis. Angiogenesis is the development of new blood vessels from pre-existing vasculature [39]. Vascular endothelial growth factor (VEGF) is a potent angiogenic factor that can also promote vasodilation of blood vessels, induce vascular permeability, and mediate migration of endothelial cells to form new blood vessel structures [40,41]. This neovasculature is known to be leaky, disorganized, and tortuous [37,41,42]. In the brain, the neovasculature is abnormal in structural components of the BBB including tight junctions and the basement membrane layer [37,42]. Another mechanism by which melanoma cells acquire blood supply is vessel co-option. Vessel co-option is the use of pre-existing blood vessels, whereby cells are directly associated with and grow along blood

vessels; this mechanism of vascularization is quite common in brain tumors [42–45]. Finally, there is vasculogenic mimicry. This is where tumor cells line vascular walls rather than endothelial cells [46,47]. The end results are vessel-like networks that mimic normal or embryonic-like vessel structures [39]. The term 'vasculogenic mimicry' was first introduced in 1999 and was first described in melanoma, more specifically in uveal and metastatic cutaneous melanomas, in which patterned microvasculature consisting of networks and loops or looping networks were observed [46,47].

Vessel co-option does not cause disturbance to the endothelium of the BBB [21,24] and the barrier remains intact. This might explain why some metastases in our study did not enhance after administration of Gd-DTPA. There is also the possibility that vasculogenic mimicry can also be contributing toward the lack of enhancement of brain metastases after Gd-DTPA administration. Van der Schaft *et al.* [48] showed that melanoma tumors that exhibited evidence of vasculogenic mimicry were relatively unaffected by antiangiogenic treatments, suggesting that tumor cell-lined vasculature was impenetrable or unresponsive to angiogenic inhibitors.

Oliver *et al.* [49] have shown that VEGF secretions are associated with the A2058 melanoma cell line, and Leenders *et al.* [28] observed VEGF expression in melanoma brain metastases that showed vessel co-option. It is possible that VEGF secretion by melanoma cells co-opted to blood vessels in the brain and VEGF-induced angiogenesis may be simultaneously contributing to leakiness of the BBB [28,37]. Angiogenesis, vessel co-option, and vasculogenic mimicry [39,42–45,46,47] may be occurring simultaneously and together could influence or control the permeability status of individual brain metastases.

## Conclusion

Clinically, T1wSE with Gd-DTPA administration is the gold standard for brain tumor imaging [36,50]. Findings from our characterized, clinically relevant model reveal that some metastases may go undetected on T1wSE imaging and that using bSSFP imaging enables the detection of nonenhancing brain metastases at early time points. Additional longitudinal studies assessing the molecular and biochemical properties of enhancing and nonenhancing metastases will be an important factor in understanding permeability behavior, disease progression, and variable responses of melanoma brain metastases to treatments.

## Acknowledgements

The authors would like to thank Felicia Simedrea for her skilled expertise and assistance with intracardiac cell injections. An extended thank you also goes to Catherine McFadden and Yuhua Chen for their help with the preparation as well as the maintenance of the human

melanoma cell line, and the histological portion of the study, respectively.

### Conflicts of interest

There are no conflicts of interest.

### References

- Fife KM, Colman MH, Stevens GN, Firth IC, Moon D, Shannon KF, et al. Determinants of outcome in melanoma patients with cerebral metastases. *J Clin Oncol* 2004; **22**:1293–1300.
- Byrne TN, Cascino TL, Posner JB. Brain metastasis from melanoma. *J Neurooncol* 1983; **1**:313–317.
- Amer MH, Al-Sarraf M, Baker LH, Vaitkevicius VK. Malignant melanoma and central nervous system metastases: incidence, diagnosis, treatment and survival. *Cancer* 1978; **42**:660–668.
- Madajewicz S, Karakousis C, West CR, Caracandas J, Avellanosa AM. Malignant melanoma brain metastases. Review of Roswell Park Memorial Institute experience. *Cancer* 1984; **53**:2550–2552.
- Chason JL, Walker FB, Landers JW. Metastatic carcinoma in the central nervous system and dorsal root ganglia. A prospective autopsy study. *Cancer* 1963; **16**:781–787.
- McNeer G, Das Gupta T. Problem of recurrence in the management of melanoma. *CA Cancer J Clin* 1965; **15**:270–274.
- Eichler AF, Loeffler JS. Multidisciplinary management of brain metastases. *Oncologist* 2007; **12**:884–898.
- Raizer JJ, Hwu WJ, Panageas KS, Wilton A, Baldwin DE, Bailey E, et al. Brain and leptomeningeal metastases from cutaneous melanoma: survival outcomes based on clinical features. *Neuro Oncol* 2008; **10**:199–207.
- Zimm S, Wampler GL, Stablein D, Hazra T, Young HF. Intracerebral metastases in solid-tumor patients: natural history and results of treatment. *Cancer* 1981; **48**:384–394.
- Salvati M, Frati A, D'Elia A, Pescatori L, Piccirilli M, Pietrantonio A, et al. Single brain metastases from melanoma: remarks on a series of 84 patients. *Neurosurg Rev* 2012; **35**:211–217, Discussion 217–8.
- Soffietti R, Rudà R, Mutani R. Management of brain metastases. *J Neurol* 2002; **249**:1357–1369.
- Ellerhorst J, Strom E, Nardone E, McCutcheon I. Whole brain irradiation for patients with metastatic melanoma: a review of 87 cases. *Int J Radiat Oncol Biol Phys* 2001; **49**:93–97.
- Norden AD, Wen PY, Kesari S. Brain metastases. *Curr Opin Neurol* 2005; **18**:654–661.
- Dvorak HF, Nagy JA, Dvorak JT, Dvorak AM. Identification and characterization of the blood vessels of solid tumors that are leaky to circulating macromolecules. *Am J Pathol* 1988; **133**:95–109.
- Zhang C, Yu D. Microenvironment determinants of brain metastasis. *Cell Biosci* 2011; **1**:8.
- Gerstner ER, Fine RL. Increased permeability of the blood–brain barrier to chemotherapy in metastatic brain tumors: establishing a treatment paradigm. *J Clin Oncol* 2007; **25**:2306–2312.
- Sarin H, Kanevsky AS, Fung SH, Butman JA, Cox RW, Glen D, et al. Metabolically stable bradykinin B2 receptor agonists enhance transvascular drug delivery into malignant brain tumors by increasing drug half-life. *J Transl Med* 2009; **7**:33.
- Lockman PR, Mittapalli RK, Taskar KS, Rudraraju V, Gril B, Bohn KA, et al. Heterogeneous blood-tumor barrier permeability determines drug efficacy in experimental brain metastases of breast cancer. *Clin Cancer Res* 2010; **16**:5664–5678.
- Percy DB, Ribot EJ, Chen Y, McFadden C, Simeone C, Steeg PS, et al. In vivo characterization of changing blood–tumor barrier permeability in a mouse model of breast cancer metastasis: a complementary magnetic resonance imaging approach. *Invest Radiol* 2011; **46**:718–725.
- Zhang RD, Price JE, Fujimaki T, Bucana CD, Fidler IJ. Differential permeability of the blood-brain barrier in experimental brain metastases produced by human neoplasms implanted into nude mice. *Am J Pathol* 1992; **141**:1115–1124.
- Leenders W, Küsters B, Pikkemaat J, Wesseling P, Ruiter D, Heerschap A, et al. Vascular endothelial growth factor-A determines detectability of experimental melanoma brain metastasis in GD-DTPA-enhanced MRI. *Int J Cancer* 2003; **105**:437–443.
- Schellenberg AE, Buist R, Del Bigio MR, Toft-Hansen H, Khoroshi R, Owens T, Peeling J. Blood–brain barrier disruption in CCL2 transgenic mice during pertussis toxin-induced brain inflammation. *Fluids Barriers CNS* 2012; **9**:10.
- Rodgers J, McCabe C, Gettinby G, Bradley B, Condon B, Kennedy PG. Magnetic resonance imaging to assess blood–brain barrier damage in murine trypanosomiasis. *Am J Trop Med Hyg* 2011; **84**:344–350.
- Budde MD, Gold E, Jordan EK, Frank JA. Differential microstructure and physiology of brain and bone metastases in a rat breast cancer model by diffusion and dynamic contrast enhanced MRI. *Clin Exp Metastasis* 2012; **29**:51–62.
- Starr JM, Farrall AJ, Armitage P, McGurn B, Wardlaw J. Blood-brain barrier permeability in Alzheimer's disease: a case-control MRI study. *Psychiatry Res* 2009; **171**:232–241.
- Wang F, Cheng Y, Mei J, Song Y, Yang YQ, Liu Y, Wang Z. Focused ultrasound microbubble destruction-mediated changes in blood–brain barrier permeability assessed by contrast-enhanced magnetic resonance imaging. *J Ultrasound Med* 2009; **28**:1501–1509.
- Kassner A, Thornhill RE, Liu F, Winter PM, Caruthers SD, Wickline SA, Lanza GM. Assessment of tumor angiogenesis: dynamic contrast-enhanced MRI with paramagnetic nanoparticles compared with Gd-DTPA in a rabbit Vx-2 tumor model. *Contrast Media Mol Imaging* 2010; **5**:155–161.
- Leenders WP, Küsters B, Verrijp K, Maass C, Wesseling P, Heerschap A, et al. Antiangiogenic therapy of cerebral melanoma metastases results in sustained tumor progression via vessel co-option. *Clin Cancer Res* 2004; **10** (18 Pt 1):6222–6230.
- Sundström T, Daphu I, Wendelbo I, Hodneland E, Lundervold A, Immervoll H, et al. Automated tracking of nanoparticle-labeled melanoma cells improves the predictive power of a brain metastasis model. *Cancer Res* 2013; **73**:2445–2456.
- Morsi A, Gaziel-Sovran A, Cruz-Munoz W, Kerbel RS, Golfinos JG, Hernando E, Wadghiri YZ. Development and characterization of a clinically relevant mouse model of melanoma brain metastasis. *Pigment Cell Melanoma Res* 2013; **26**:743–745.
- Thorsen F, Fite B, Mahakian LM, Seo JW, Qin S, Harrison V, et al. Multimodal imaging enables early detection and characterization of changes in tumor permeability of brain metastases. *J Control Release* 2013; **172**:812–822.
- Heyn C, Ronald JA, Ramadan SS, Snir JA, Barry AM, MacKenzie LT, et al. In vivo MRI of cancer cell fate at the single-cell level in a mouse model of breast cancer metastasis to the brain. *Magn Reson Med* 2006; **56**:1001–1010.
- Isiklar I, Leeds NE, Fuller GN, Kumar AJ. Intracranial metastatic melanoma: correlation between MR imaging characteristics and melanin content. *AJR Am J Roentgenol* 1995; **165**:1503–1512.
- Smith AB, Rushing EJ, Smirniotopoulos JG. Pigmented lesions of the central nervous system: radiologic–pathologic correlation. *Radiographics* 2009; **29**:1503–1524.
- Escott EJ. A variety of appearances of malignant melanoma in the head: a review. *Radiographics* 2001; **21**:625–639.
- Gaviani P, Mullins ME, Braga TA, Hedley-Whyte ET, Halpern EF, Schaefer PS, Henson JW. Improved detection of metastatic melanoma by T2\*-weighted imaging. *Am J Neuroradiol* 2006; **27**:605–608.
- Jain RK, di Tomaso E, Duda DG, Loeffler JS, Sorensen AG, Batchelor TT. Angiogenesis in brain tumours. *Nat Rev Neurosci* 2007; **8**:610–622.
- Folkman J. What is the evidence that tumors are angiogenesis dependent? *J Natl Cancer Inst* 1990; **82**:4–6.
- Döme B, Hendrix MJ, Paku S, Tóvári J, Timár J. Alternative vascularization mechanisms in cancer: Pathology and therapeutic implications. *Am J Pathol* 2007; **170**:1–15.
- Ellis LM, Hicklin DJ. VEGF-targeted therapy: mechanisms of anti-tumour activity. *Nat Rev Cancer* 2008; **8**:579–591.
- Dvorak HF, Brown LF, Detmar M, Dvorak AM. Vascular permeability factor/vascular endothelial growth factor, microvascular hyperpermeability, and angiogenesis. *Am J Pathol* 1995; **146**:1029–1039.
- Rubenstein JL, Kim J, Ozawa T, Zhang M, Westphal M, Deen DF, Shuman MA. Anti-VEGF antibody treatment of glioblastoma prolongs survival but results in increased vascular cooption. *Neoplasia* 2000; **2**:306–314.
- Leenders WP, Küsters B, de Waal RM. Vessel co-option: how tumors obtain blood supply in the absence of sprouting angiogenesis. *Endothelium* 2002; **9**:83–87.
- Holash J, Maisonpierre PC, Compton D, Boland P, Alexander CR, Zagzag D, et al. Vessel cooption, regression, and growth in tumors mediated by angiotensin and VEGF. *Science* 1999; **284**:1994–1998.
- Kienast Y, von Baumgarten L, Fuhrmann M, Klinkert WE, Goldbrunner R, Herms J, Winkler F. Real-time imaging reveals the single steps of brain metastasis formation. *Nat Med* 2010; **16**:116–122.
- Maniatis AJ, Folberg R, Hess A, Seftor EA, Gardner LM, Pe'er J, et al. Vascular channel formation by human melanoma cells in vivo and in vitro: vasculogenic mimicry. *Am J Pathol* 1999; **155**:739–752.

- 47 Hendrix MJ, SefTOR EA, Hess AR, SefTOR RE. Vasculogenic mimicry and tumour-cell plasticity: lessons from melanoma. *Nat Rev Cancer* 2003; **3**:411–421.
- 48 Van der Schaft DW, SefTOR RE, SefTOR EA, Hess AR, Gruman LM, Kirschmann DA, *et al.* Effects of angiogenesis inhibitors on vascular network formation by human endothelial and melanoma cells. *J Natl Cancer Inst* 2004; **96**:1473–1477.
- 49 Oliver VK, Patton AM, Desai S, Lorang D, Libutti SK, Kohn EC. Regulation of the pro-angiogenic microenvironment by carboxyamido-triazole. *J Cell Physiol* 2003; **197**:139–148.
- 50 Anzalone N, Gerevini S, Scotti R, Vezzulli P, Picozzi P. Detection of cerebral metastases on magnetic resonance imaging: intraindividual comparison of gadobutrol with gadopentetate dimeglumine. *Acta Radiol* 2009; **50**:933–940.